Journal of Membrane Science 382 (2011) 252–261

Contents lists available at ScienceDirect

Journal of Membrane Science

journal homepage: www.elsevier.com/locate/memsci

Optimization and characterization of electroless co-deposited PdRu membranes: Effect of the plating variables on morphology

Fernando Braun, Ana M. Tarditi, Laura M. Cornaglia*

Instituto de Investigaciones en Catálisis y Petroquímica (FIQ, UNL-CONICET), Santiago del Estero 2829, 3000 Santa Fe, Argentina

ARTICLE INFO

Article history:
Received 20 May 2011
Received in revised form 10 July 2011
Accepted 9 August 2011
Available online 17 August 2011

Keywords:
PdRu membrane
Electroless plating
Co-deposition

ABSTRACT

PdRu films were successfully synthesized on top of non-porous stainless steel supports by electroless co-deposition. The effect of synthesis variables on morphology, substrate adherence, bulk and surface composition was studied. The microstructure and morphology of the samples were analyzed by X-ray diffraction and scanning electron microscopy. Homogeneous and defect-free PdRu films were obtained employing baths at low pH, moderate to high agitation speeds, high concentration of hydrazine, using EDTA as a stabilizer and temperatures near 50 °C. Films characterized by X-ray photoelectron spectroscopy showed Pd segregation after annealing the sample at 400 °C in H_2 (5%)/Ar in the load-lock chamber of the spectrometer. The optimized conditions were employed to synthesize a PdRu composite membrane on top of a tubular porous stainless steel substrate (0.1 μm grade). Hydrogen permeation was measured over a 350–450 °C temperature range and a trans-membrane pressure up to 100 kPa. The PdRu membrane showed good performance with a hydrogen permeability of 6.5×10^{-9} mol m^{-1} s^{-1} $Pa^{-0.5}$ and a selectivity higher than 1700.

1. Introduction

Due to the increasing energy demand and high levels of pollution generated by the existing energy-producing technologies, it is necessary to look for and use new eco-friendly energy sources or carriers. In this context, hydrogen appears as an energy carrier that can be used in internal combustion engines or fuel cells, avoiding unwanted emissions. However, one of the main disadvantages of H_2 for use in low temperature fuel cells is the presence of impurities such as CO, CO_2 and hydrocarbons from reforming reactions. A well-known technology for hydrogen purification is the use of metallic Pd and Pd-alloy membrane reactors at both laboratory and pilot plant scale, which allows increasing the levels of reaction conversion and capture of CO_2.

The use of Pd membranes for hydrogen purification has decreased due to the high cost of the membranes and to the embrittlement produced by their exposure to H_2 at temperatures below 300 °C. In order to avoid these problems, binary alloys have been developed. It has been reported that certain binary alloys such as PdAu and PdCu improve membrane properties, e.g. resistance to contaminants (CO and H_2S), while others such as PdAg improve hydrogen permeability [1–4].

The synthesis of Ru and PdRu films for application in membranes for hydrogen separation has not been widely studied [5–10]. Through SEM, Gryaznov and co-workers [7] studied the influence of temperature and atmosphere over 100 μm thick $Pd_{94}Ru_6$ alloy foils. These authors reported crevices formed in foils annealed 2 h at 200 °C in vacuum or H_2, these gaps being larger in the reduction atmosphere by a factor of 3–5. Besides, Way and co-workers [8] synthesized uniform $PdRu_{4.5-10}$ composite membranes by co-deposition. They reported an increase of 78% in the film hardness compared to pure Pd using a PdRu film with 7.2% Ru; all membranes showed similar permeation to pure Pd. Ryi et al. [10] studied the effect on membrane performance of a Ru thin layer deposited on top of Pd/Al_2O_3-SS by sequential deposition. Using a membrane with low Ru composition, the latter authors reported an enhancement of 40% in hydrogen permeability compared with a Pd/Al_2O_3-SS membrane. Ma and co-workers [9] showed a steady decline in hydrogen permeability due to Pd film contamination with stainless steel metals in a Pd/SS membrane using 0.5 μm of Ru as a diffusion barrier. Wang et al. [11] synthesized a $Pd_{69}Ag_{30}Ru_1/\alpha$-$Al_2O_3$ membrane by electroless co-deposition. The authors reported hydrogen permeability three times higher than with a PdAg membrane and about four times higher than a Pd membrane.

On the other hand, catalytic results of PdRu membrane reactors have also been published [12–14]. Nam et al. [12] studied the methane steam reforming reaction in a membrane reactor made of a $Pd_{94}Ru_6$ tube 100 μm thick. Methane conversion was improved as high as 80% in the membrane reactor and almost complete conversion could be obtained at 600 °C.

Alloy or non-alloy bimetallic films could be synthesized by sequential or simultaneous deposition. The synthesis of the PdAg

* Corresponding author. Tel.: +54 342 4536861.
E-mail address: lmcornag@fiq.unl.edu.ar (L.M. Cornaglia).

0376-7388/$ – see front matter © 2011 Elsevier B.V. All rights reserved.
doi:10.1016/j.memsci.2011.08.019

alloy has been widely studied in the Pd-alloy membrane area. This alloy has been synthesized by sequential [15–19] and simultaneous [20–24] deposition using the electroless plating technique. Different annealing strategies have been used for both routes of deposition in order to obtain homogeneous composition alloys. Films obtained by sequential deposition need stronger heat treatments, longer times or higher temperatures compared with films obtained by co-deposition. These severe treatments cause diffusion of stainless steel metals and losses of permeability [25,26]. However, simultaneous deposition presents certain difficulties in obtaining films with homogeneous morphology and desired bulk composition.

Due to the advantages of using electroless deposition in the synthesis of binary and ternary Pd alloys membranes, the influence of synthesis variables on the quality of the film should be studied. Ayturk and Ma [27] analyzed the influence of temperature, hydrazine, palladium and silver concentration, and stirring rate on the Pd and Ag deposition kinetics. These authors reported that the electroless plating of both Pd and Ag was strongly affected by the external mass transfer in the absence of bath agitation. Yeung and co-workers [20] reported the proper conditions for co-deposition of palladium and silver from a mixed plating bath. The authors studied the Pd/Ag molar ratio, hydrazine, total metal and ammonium hydroxide concentration effect on plating rate and film properties such as composition and microstructure. To synthesize Pd membranes with 0–10 wt.% ruthenium, Gade et al. [8] employed a carbonless co-deposition bath to avoid carbon contamination in the finished film.

This study presents a detailed analysis of the influence of different plating variables as bath temperature, pH and stirring rate on morphology, substrate adherence, bulk and surface composition of co-deposited PdRu films. PdRu films were fabricated by simultaneous electroless plating supported on top of non-porous discs and on both porous stainless steel discs and tubes. Surface composition and segregation of PdRu films were studied by X-ray Photoelectron Spectroscopy (XPS) and Angle Resolved XPS. For the PdRu tubular membrane, hydrogen flux measurements were performed during the annealing stage at 500 °C. After this treatment, the H_2 permeation was measured between 350 and 450 °C up to a 100 kPa pressure difference.

2. Experimental

2.1. PdRu films deposition optimization

PdRu films were deposited by simultaneous electroless plating on top of non-porous stainless steel 316L discs (NPSSD) of 0.9 cm in diameter and 0.2 cm thickness. Before the metal deposition, discs were polished with 380, 500, 800, 1000 and 1200 grit sandpapers and finally with a ~1 μm-grade paste and with a suspension of γ-alumina (50 nm). After grinding, the discs were immersed in a mixed solution of concentrated HCl (37 wt.%) and concentrated HNO_3 (69 wt.%) during 5 min in order to create surface rugosity [28]. The molar ratio of [HCl] to [HNO_3] employed was 1.6. Finally, the discs were washed with an alkaline solution consisting of 0.12 M $Na_3PO_4{\cdot}12\ H_2O$, 0.6 M Na_2CO_3 and 1.12 M NaOH using the procedure reported by Ma et al. [29] and calcined 12 h at 500 °C. Prior to the electroless plating, the discs were activated. The sensitizing-activation of the substrate was conducted in an acidic $SnCl_2$ (1 g/l) solution followed by an acidic $PdCl_2$ solution (0.1 g/l) at room temperature. The sensitizing-activation process was repeated six times. After the substrate was pre-seeded with Pd nuclei, the simultaneous electroless plating was carried out by immersing the disc into a plating bath containing Pd and Ru. After the first three 1 h co-depositions, the activation process was repeated three times.

The conditions and concentrations of the solutions used in the activation, modification of pH and plating baths are detailed in Table 1. The plating bath solution used in the PdRu co-deposition was obtained by mixing a palladium complex with ruthenium solutions, maintaining a total metal concentration of 10 mM in all the experiments.

In the pH effect study a solution of NaOH was used as a pH modifier. In order to obtain a curve (not shown) of the pH vs. volume of NaOH, different amounts of alkaline solution were added to the PdRu plating bath. For the bath agitation a magnetic stirrer was used to regulate the agitation rate, measured in revolutions per minute (rpm) up to 800 rpm. The disodium ethylenediaminetetraacetic acid (EDTA) effect on the PdRu deposition rate and film morphology was also studied. The hydrazine concentration was studied at 10 mM and 30 mM being in excess in both cases compared with the metal total concentration. The palladium and ruthenium redox reactions involved in the electroless co-deposition are presented below:

$$2Pd(NH_3)_4^{+2} + N_2H_4 + 4OH^- \rightarrow 2Pd + N_2\uparrow + 4H_2O + 8NH_3 \quad (1)$$

$$4Ru^{+3} + 3N_2H_4 + 12OH^- \rightarrow 4Ru + 3N_2\uparrow + 12H_2O \quad (2)$$

All the experiments were carried out with a volume of plating bath/support area ratio equal to 5.7 cm^3/cm^2. The thickness was calculated from the disc weight gain and the density of Pd and Ru.

2.2. PdRu membrane preparation and permeation measurements

A porous stainless steel tube 0.1 μm grade (PSST, 0.64 cm i.d. and 0.95 cm o.d.) and a porous stainless steel disc 0.2 μm grade (PSSD, 1.27 cm in diameter and thickness of 2 mm) were used as supports of the PdRu membranes. The supports were purchased from Mott Metallurgical Corporation. Prior to any plating experiment, they were cleaned with the same procedure used for the non-porous supports. After that, the tube and disc were oxidized at 500 °C for 12 h. In order to avoid intermetallic diffusion between the stainless steel elements and the PdRu alloy, the supports were modified with alumina by means of the dip coating vacuum assisted method [30]. The activation sequence used for both substrates was the same used in the optimization stage for the non-porous supports.

Prior to the PdRu co-deposition on top of the tubular support, two 1 h depositions of Pd were performed in order to achieve a uniform surface. Palladium and ruthenium were deposited by simultaneous electroless deposition using the previously optimized conditions: $T = 50$ °C, $[N_2H_4] = 30$ mM, [EDTA] = 180 mM, [Ru] = 1 mM, no stirring. The volume of plating bath/surface area ratio was 4.7 cm^3/cm^2. The synthesis procedure was repeated until the composite membrane became impermeable to N_2 at room temperature and at a pressure difference of 10 kPa. The film thickness was estimated from the weight gain after metal deposition and checked by SEM.

Thermal treatments and gas permeation measurements were conducted in a shell-and-tube membrane module [25]. The sample was then heated up to 500 °C in a H_2 atmosphere in order to promote metallic inter-diffusion, homogeneous metals composition and permeation stabilization. The temperature was increased from room temperature up to 500 °C with a heating rate of 0.5 °C min^{-1} in nitrogen flow and then, the annealing process was conducted in hydrogen atmosphere and a trans-membrane pressure of 10 kPa. The membrane module was placed in an electrical furnace and heated at different temperatures. All the gases were fed to the permeator using calibrated mass-flow controllers. Feed gases flowed along the outside of the membrane and the permeated gases were measured in the inner side of the membrane. A N_2 sweep gas stream was introduced in the permeated side only during the annealing process. Pressure differences across the membranes

Table 1
Chemical composition of Pd and Ru electroless plating solutions, activation and plating conditions.

	Activation/pH modifier	Plating bath	
		Pd	Ru
$SnCl_2$ (g/l)	1	–	–
$PdCl_2$ (g/l)	0.10	–	–
HCl (M)	1	–	–
NaOH (g/l)	102	–	–
Hydrazine (mM)	–	10/30	
28–30% NH_4OH (M)	–	9.85	–
Na_2EDTA (mM)	–	180	–
$PdCl_2$ (mM)	–	20.30	–
HCl (mM)	–	–	0.12
$RuCl_3{\cdot}3H_2O$ (mM)	–	–	3.08
pH	–	11.5–14	
Temperature (°C)	–	30–80	

were obtained using a back-pressure regulator to vary the pressure on the upstream side and keeping the pressure constant downstream at 100 kPa. The gas permeation rates were measured using two bubble flow meters at room temperature and pressure.

2.3. Film characterization

2.3.1. X-ray diffraction

The phase structure of the samples was determined by X-ray diffraction. The XRD patterns of the films were obtained with an XD-D1 Shimadzu instrument, using Cu Kα ($\lambda = 1.542$ Å) radiation at 30 kV and 40 mA. The scan rate was 1–2° min^{-1} in the range $2\theta = 15$–90°.

2.3.2. Scanning electron microscopy and energy-dispersive X-ray analysis

The outer surface and cross-section images of the samples were obtained using a Zeiss FEG-SEM instrument, model SUPRA 40, equipped with an energy dispersive analytical system (Oxford Instruments). For the cross-section views, the discs were placed into a plastic tube; then epoxy resin was added. After hardening, they were cut in halves. The grinding was carried out with waterproof abrasive paper of 180, 280, 500, 800 and 1200 grit. The polishing was done with a ~1 μm-grade paste, and finally with a suspension of γ-alumine (50 nm). The grinding and the polishing cycles lasted 5 min; after each cycle, it was necessary to clean the samples with ethyl alcohol in ultrasonic bath.

2.3.3. X-ray photoelectron spectroscopy

XPS analyses were performed in a multi-technique system (SPECS) equipped with an Al-monochromatic X-ray source, and a hemispherical PHOIBOS 150 analyzer operating in the fixed analyzer transmission (FAT) mode. The spectra were obtained using a monochromatic Al Kα radiation ($h\upsilon = 1486.6$ eV) operated at 300 W and 14 kV. The pass energy for the element scan was 30 eV. The working pressure in the analyzing chamber was less than 5×10^{-10} kPa. The XPS analyses were performed on the annealing samples and after different treatments in the main chamber. Before introducing the samples in the main chamber of the spectrometer, they were heated in a 5% H_2/Ar mixture in the load-lock chamber. The spectra of Pd 3d, Pd 3p, O1s, C 1s, Ru 3d, Ru 3p, Fe 2p were recorded for each sample. The data treatment was performed with the Casa XPS program (Casa Software Ltd, UK). The peak areas were determined by integration employing a Shirley-type background. Peaks were considered to be a mixture of Gaussian and Lorentzian functions. For the quantification of the elements, we used the sensitivity factors provided by the manufacturer.

In order to study the effect of different annealing treatments on surface segregation, the XPS spectra of Pd and Ru were recorded at room temperature after annealing the sample at different temperatures in situ in the main chamber.

2.3.4. Angle resolved X-ray spectroscopy

By varying the take-off angle between the direction of the escaping photoelectron and the surface plane of the sample, it was possible to obtain the surface segregation trend in the near-surface region. The measurements under different angles were carried out by tilting the sample with respect to the analyzer. For each ARXPS experiment, measurements were performed at six different angles up to 60° to the surface normal. All spectra were taken in medium area mode, with a spot area of about 3 mm.

3. Results and discussion

3.1. Plating bath variables

This section presents the results obtained from studying the influence of the plating variables as pH, bath temperature, $[N_2H_4]$ and stirring rate on the deposition rate, morphology and film composition.

3.1.1. pH effect on PdRu deposit morphology

The influence of pH in the plating bath on PdRu film deposition rate and morphology has not been previously reported. In this work the effect of pH was studied between 11.5 and 14, using a NaOH solution as a pH modifier.

A decrease in PdRu film thickness and bulk precipitation was observed by increasing the pH above 11.5 (Fig. 1). This could be due to the instability of the plating bath with the addition of NaOH. The micrographs in Fig. 2 show the surface morphology of the PdRu film obtained at pH 11.50, 12.75 and 14, respectively. By increasing pH, a reduction in film adhesion to the substrate and more heterogeneous morphologies were obtained. The PdRu film synthesized at the highest pH value showed regions where the non-porous substrate was not covered, which could be produced by film detachment or no deposition. Therefore, the lowest pH value (pH = 11.5) was selected to study the effect of agitation rate, hydrazine concentration, plating temperature, EDTA and Ru/Metal ratio. At pH lower than 11.5, Pd bulk precipitation could be produced. Yeung et al. [31] studied the effect of ammonium hydroxide concentration on the Pd plating rate. These authors observed a decrease in the plating rate when increasing the ammonium hydroxide concentration and Pd bulk precipitation at low ammonium hydroxide concentration.

3.1.2. Bath stirring effect on deposition rate and film morphology

With the aim of reducing mass transfer limitation on the electroless plating kinetics and to improve the deposition morphology of PdRu films, the co-deposition was performed by stirring the plating

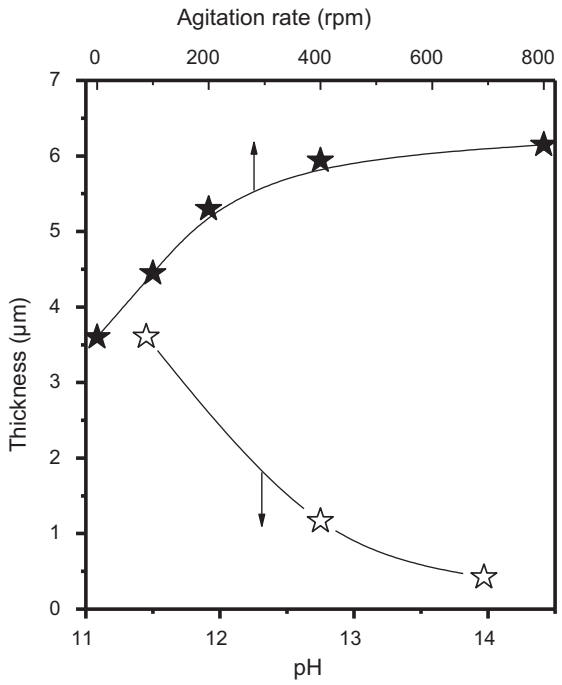

Fig. 1. pH and agitation rate effect on the thickness of the PdRu samples. Synthesis conditions: [Pd + Ru] = 10 mM, [Ru] = 1 mM, T = 50 °C, [N_2H_4] = 30 mM, [EDTA] = 180 mM. Three 1 h co-depositions.

bath. Fig. 1 shows the co-deposition plating rate measured as thickness obtained in three 1 h depositions as a function of the agitation rate. The results show a significant influence of bath agitation on the deposition rate. An increase in thickness is obtained by increasing the agitation rate, from 3.6 μm for the non-stirred sample up to 6 μm for the sample synthesized at 800 rpm. The non-agitated plating bath presents an external mass transfer limitation, as evidenced by the increase in thickness when increasing the stirring rate. Comparing micrographs of the samples agitated at 200 and 800 rpm (Fig. 3b and c), a decrease in the size and number of pores onto the surface of the PdRu film is observed. As shown in Fig. 1, no further effect was observed beyond 400 rpm, probably due to the fact that the PdRu co-deposition is controlled by the chemical reaction kinetics.

Ayturk and Ma [27] studied the deposition kinetics of Pd and Ag by electroless plating in agitated plating baths. In the case of Pd plating, at an agitation rate of 200 rpm and even more at 400 rpm, the micrographs suggested that the Pd deposition was noticeably more uniform and smooth. The SEM images of the Ag deposits at a rate of 100 rpm showed more uniform clusters in comparison to the regular Ag deposition morphology (rpm = 0), which consisted of randomly distributed clusters with different shapes and sizes. The authors claimed that the uniform Pd and Ag deposition morphology was originated from the fast nucleation rates achieved in the presence of agitation [29].

3.1.3. EDTA effect on PdRu deposition rate and morphology

To avoid carbon contamination from EDTA and improve the efficiency of synthesis, similar experiments were performed at 50 °C with and without EDTA, varying hydrazine concentration and Ru/M ratio.

Fig. 4 shows the thickness obtained at two hydrazine concentrations (30 mM and 10 mM) and at a [Ru] = 1 mM, with and without EDTA. In both cases, a decrease in thickness by decreasing the concentration of hydrazine is obtained, this behavior being more evident in the absence of EDTA. A slight decrease in the thickness of PdRu co-deposited films were obtained by increasing the Ru/M ratio from 0.1 to 0.2 at an [N_2H_4] = 30 mM.

SEM surface analysis provides information whether the co-deposition of metals is limited by the mass transfer, the kinetics of reaction or by a combination of both. Dendritic or non-uniform

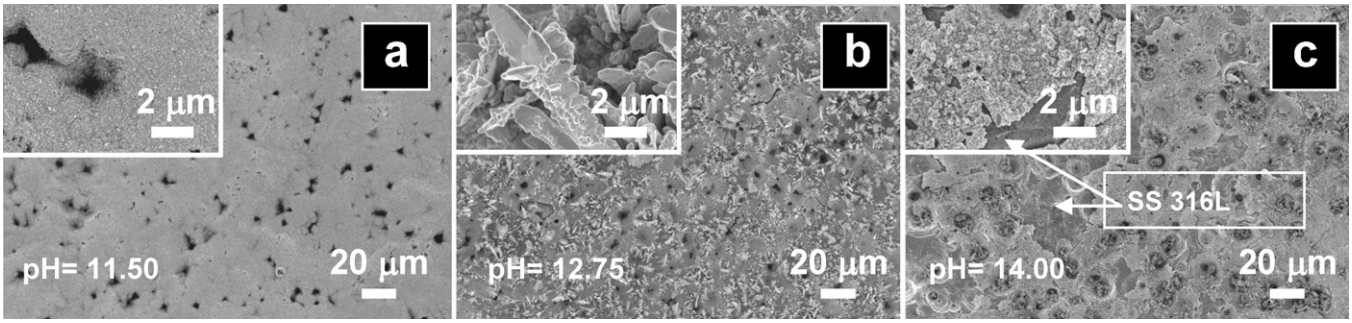

Fig. 2. pH effect on the PdRu film morphology: (a) pH = 11.50, (b) pH = 12.75 and (c) pH = 14. Synthesis conditions: [Pd + Ru] = 10 mM, [Ru] = 1 mM, T = 50 °C, [N_2H_4] = 30 mM, [EDTA] = 180 mM. Three 1 h co-depositions.

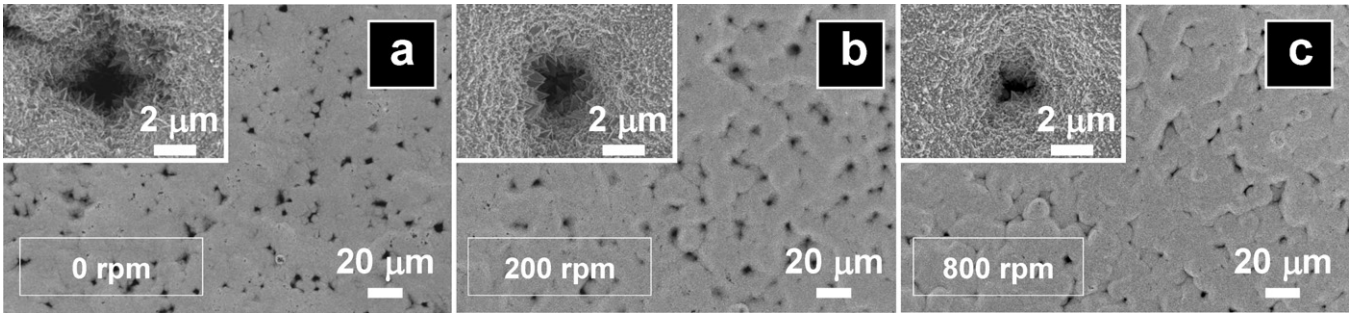

Fig. 3. Stirring rate effect on morphology. (a) 0 rpm, (b) 200 rpm and (c) 800 rpm. Synthesis conditions: [Pd + Ru] = 10 mM, [Ru] = 1 mM, T = 50 °C, [N_2H_4] = 30 mM, [EDTA] = 180 mM, pH = 11.5. Three 1 h co-depositions.

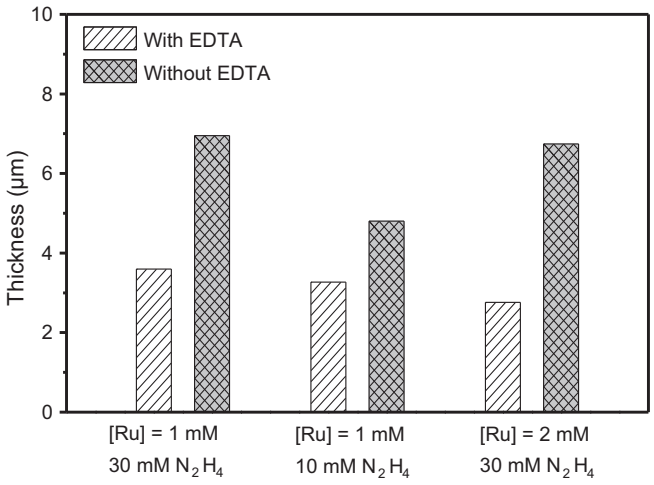

Fig. 4. Ru and hydrazine concentration effect on the thickness of the PdRu samples synthesized with and without EDTA. Synthesis conditions: [Ru + Pd] = 10 mM, T = 50 °C, [EDTA] = 180 mM, pH = 11.5. Three 1 h co-depositions.

morphologies, usually characterized by vertical growth, reflect a clear external mass transfer limitation, while uniform morphologies give an idea of chemical or mixed control [27,32]. Bhandari and Ma [32] studied the electroless and electro-plating conditions and their effect in Pd and Ag deposits morphology. By means of the linear sweep voltametry study, the authors showed that the over potential at which the Ag deposition occurred had important effects on the deposit's morphology.

Fig. 5a, c and e shows the micrographs of PdRu films synthesized with EDTA and Fig. 5b, d and f without EDTA. All samples obtained without EDTA present more heterogeneous morphologies if compared with samples prepared in the EDTA plating bath. Furthermore, micrographs of samples prepared without EDTA showed cracks, as shown in Fig. 5b. PdRu films obtained in an EDTA-free plating bath with higher concentrations of hydrazine and different concentrations of Ru (Fig. 5b and f) have a similar dendritic morphology with growth in height, while the sample with the lowest concentration of hydrazine (Fig. 5d) has less heterogeneous morphology, probably due to a lower reaction rate. Comparing SEM images of PdRu samples obtained in an EDTA-free plating bath, it can be inferred that both samples with higher hydrazine concentration present severe mass transfer limitation. PdRu films obtained with EDTA present homogeneous morphology with slight differences between them. Similar surface morphologies of the samples

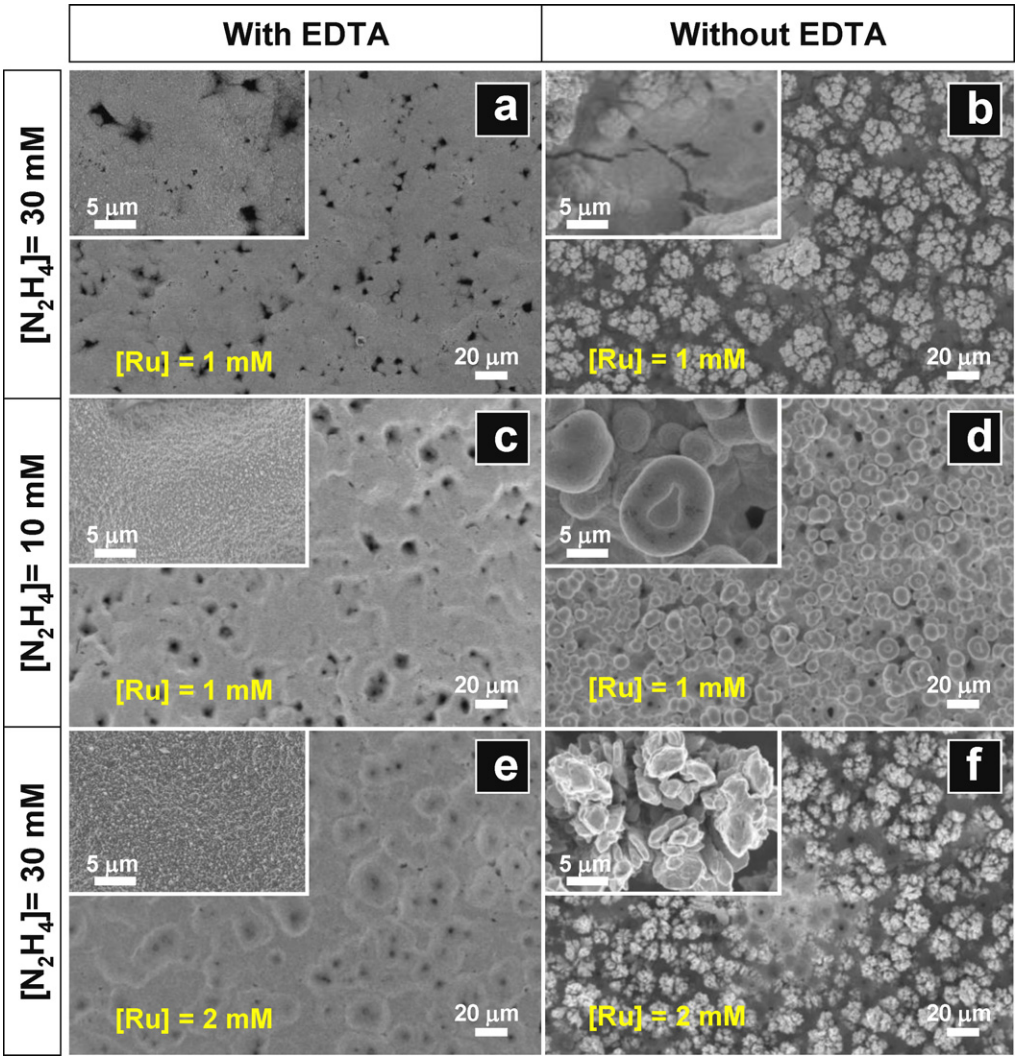

Fig. 5. Ru and hydrazine concentration effect on PdRu film morphology synthesized with EDTA (a, c and e) and without EDTA (b, d and f). Synthesis conditions: [Ru + Pd] = 10 mM, T = 50 °C, pH = 11.5. Three 1 h co-depositions.

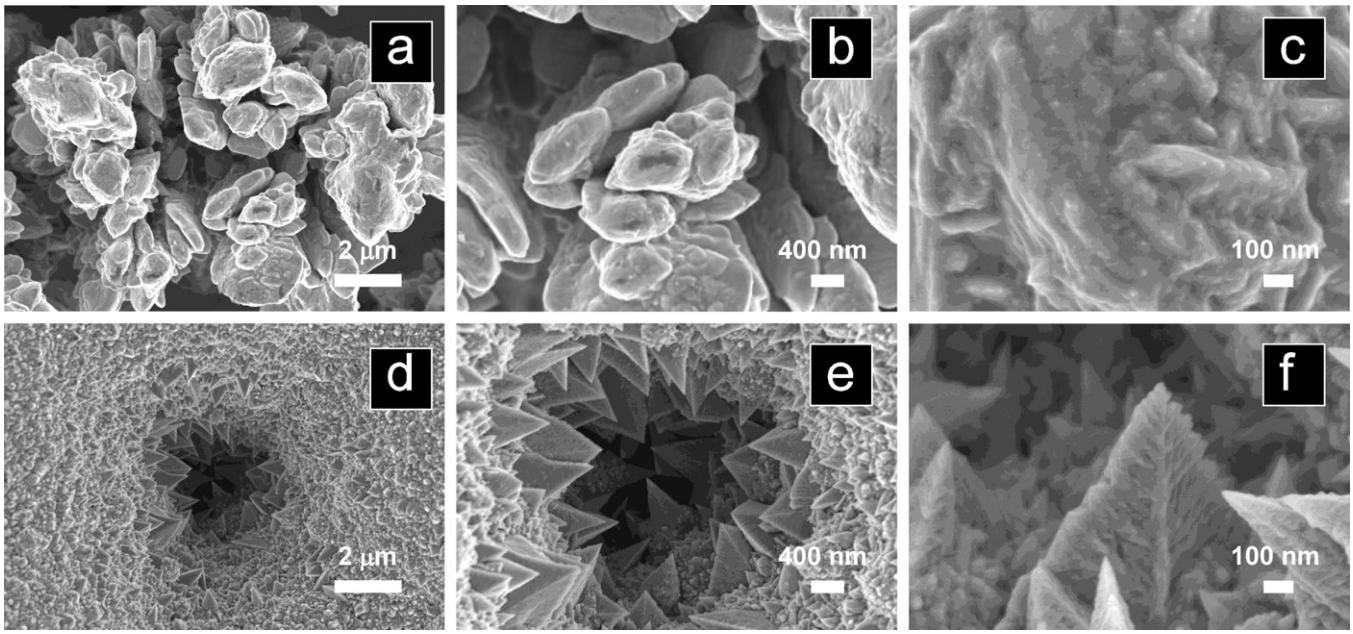

Fig. 6. High magnification SEM top-view of PdRu samples. EDTA effect on the morphology of the PdRu films synthesized without EDTA (a, b, c) and with EDTA (d, e, f).

synthesized with EDTA were observed employing a hydrazine concentration of 30 mM and 10 mM.

While results reflect an increase in the efficiency of deposition for the samples performed without EDTA, PdRu films with dendritic morphologies and cracks are obtained, as shown in Fig. 5f. This increase in thickness could be due to a lower stability of Pd and Ru in solution, compared with experiments performed with EDTA. Gade et al. [8], who also worked with carbon-free plating bath, studied palladium–ruthenium alloy membranes by electroless co-deposition. They found that the structures of the resulting PdRu films were significantly different from those of pure palladium, with larger surface features.

The high magnification SEM micrographs (Fig. 6) obtained from samples synthesized with and without EDTA can also determine whether the deposition of metals is limited by mass transfer in the kinetics of the reaction or by a combination of both. Metal films obtained without EDTA have a similar dendritic morphology, while samples obtained with EDTA (Fig. 6d, e and f), present ordered metallic structures as observed in the micrographs of the pores.

3.1.4. Temperature effect

The effect of temperature on the deposition rate of the bimetallic film was also studied. Fig. 7 shows the thicknesses obtained by varying the synthesis temperature between 30 °C and 80 °C. PdRu co-deposition rates were strongly influenced by the plating bath temperature. A significant increase of 100% in the thickness was obtained from 30 °C to 60 °C. Thickness decreased from 4 μm to 1 μm between 60 °C and 80 °C. This decrease may be due to the decomposition of hydrazine and/or a destabilization of the PdRu plating bath. These results are in complete agreement with the results reported by Ayturk and Ma [27]. The authors reported hydrazine decomposition and Pd and Ag bulk precipitation beyond 60 °C due to the instability of the electroless plating solution. Dogan and Kilicarslan [33] studied the process parameters on the synthesis of palladium membranes by electroless plating and reported a maximum in Pd deposition rate as a function of the bath temperature.

3.2. XRD phase analysis

Metallic phases were investigated by XRD. Fig. 8 shows the XRD of the non-stirred samples with and without EDTA. Two phases were detected in both films, the fcc phase of Pd and the γ-austenitic fcc phase of the support. It was not possible to estimate Ru composition by XRD data because the Ru hcp phase was not detected, probably due to the low Ru content (lower than 5% as determined by EDS). Way and co-workers [8] detected the Pd fcc phase and the Ru hcp phase in the XRD pattern of the PdRu samples synthesized by co-deposition and used the direct comparison method described by Cullity and Stock [34] to estimate the Pd composition.

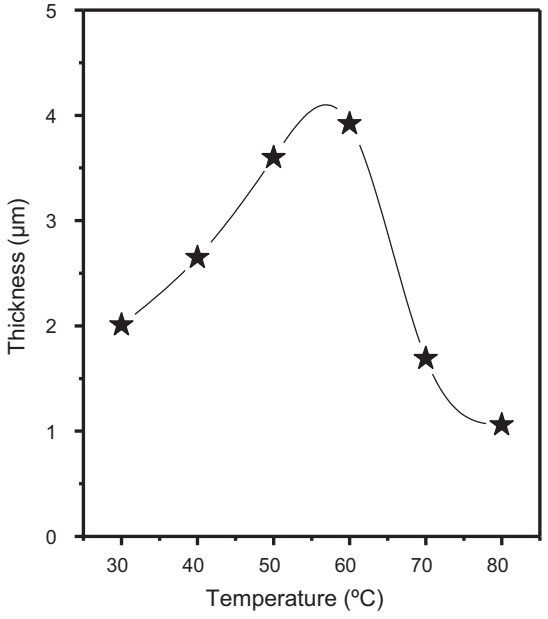

Fig. 7. Temperature effect on the thickness of the PdRu samples. Synthesis conditions: [Ru + Pd] = 10 mM, [N_2H_4] = 30 mM, [EDTA] = 180 mM, [Ru] = 1 mM, pH = 11.5. Three 1 h co-depositions.

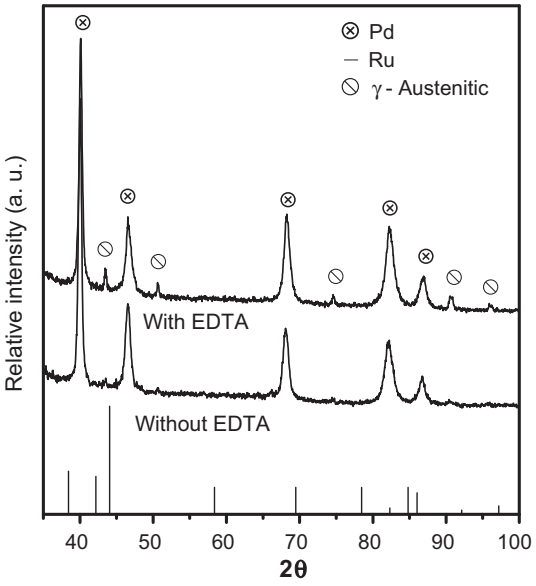

Fig. 8. X-ray diffraction patterns of the PdRu films synthesized with and without EDTA. Synthesis conditions: [Ru + Pd] = 10 mM, [%Ru] = 10, T = 50 °C, [N_2H_4] = 30 mM, [EDTA] = 180 mM, pH = 11.5. Three 1 h co-depositions.

A PdRu sample heated in H_2 at 500 °C during 24, 48 and 120 h was analyzed by XRD (Fig. 8b). The aim of this experiment was to investigate film phases during the annealing stage and the possible alloy formation. As shown in Fig. 8b only the Pd fcc phase was detected. A decrease in the FWHM peaks was observed by increasing the annealing time, which may be due to an increase of grain size, as reported by other authors for other Pd alloys [35,36]. It was not possible to detect PdRu alloy formation maybe due to the low Ru membrane composition (lower than 5% as determined by EDS).

3.3. Compositional surface analysis

In order to reveal possible surface segregation effects and oxide formation during preparation and thermal treatment, the surface chemical composition of the samples was determined using XPS. Besides Pd and Ru, the elements present before the hydrogen treatment were oxygen and carbon. The Ru/[Pd + Ru] metal ratio was 0.02–0.03 for the samples without thermal treatment. After treatment at 400 °C in the load lock chamber of the spectrometer, the Ru/[Pd + Ru] ratio decreased to 0.005. This effect may be related to the surface segregation of Pd due to its lower surface energy (Sup. Energy Pd = 1.7 J/m^2; Sup. Energy Ru = 3 J/m^2). All samples heated showed Pd segregation compared with bulk composition obtained by EDS (Table 2).

Table 2 shows the surface composition and binding energies of the Pd $3d_{5/2}$ and Ru $3d_{5/2}$ peaks for the synthesized samples after treatment in H_2 (5%)/Ar at 400 °C. Before reduction, the Ru $3d_{5/2}$ peak appears in all cases at higher binding energy showing that after synthesis the Ru was oxidized. It is important to note that after reduction, both the Pd $3d_{5/2}$ and the Ru $3d_{5/2}$ peak position could be assigned to the metallic Pd (335.1 eV) and Ru (280 eV), respectively. An influence of synthesis temperature and stirring rate on the Ru surface composition was not observed for the samples without annealing (Table 2).

To investigate the annealing temperature effect on surface composition, the PdRu 4 sample, which was not annealed ex situ up to 500 °C, was heated in the load-lock chamber of the spectrometer in H_2 (5%)/Ar at 150 °C during 10 min. After the heating, the sample was introduced into the main chamber of the spectrometer, heated up to 150 °C in vacuum during 15 min and cooled to room temperature. After that, Pd $3d_{5/2}$, Ru $3d_{5/2}$ and C 1s XPS spectra were taken. This analysis sequence was repeated every 50 °C until 500 °C. The Ru surface composition as a function of the annealing temperature is shown in Fig. 9a. A significant decrease in the Ru/[Pd + Ru] ratio was observed in the 200–250 °C temperature range, and then it remained practically unchanged at about 0.001 or lower. For this sample, the Ru surface ratio at 500 °C was lower than 0.001, while another sample annealed ex situ up to 500 °C during 24 h in H_2 stream was 0.003. The difference in those results may indicate an atmosphere effect during the annealing. A shift in binding energy and changes in the FWHM of the Pd $3d_{5/2}$ and Ru $3d_{5/2}$ peaks was not observed in the XPS spectra taken after heating at different temperatures.

As stated above, in addition to palladium and ruthenium, carbon was detected on the surface even after the thermal treatment, which could be related to contamination from the EDTA used as a complex agent. Previous publications [38,39] have reported that carbon contamination in the Pd alloy composite membrane could promote losses in permeability and selectivity. In order to have a better indication of the extent of C into the PdRu film, ARXPS experiments were performed after the in situ annealing of the PdRu7 sample at 450 °C. At this point, the Ru surface concentration was just under the detection limit of the spectrometer and Ru quantification could not be performed. In Fig. 9b, Pd and C relative compositions are represented as a function of the emission angle. The results showed an increment of the C composition by increasing the emission angle (more surface sensitive). The reason for this behavior could be assigned to the fact that the sample presents high carbon bulk content and, when the temperature increases, carbon migrates to the surface as previously reported for Pd single crystals annealing in situ in a UHV-chamber [40].

In order to corroborate the extent of C contamination, another PdRu sample was annealed ex situ during 120 h at 500 °C in H_2 stream before the XPS experiments. Even after reduction in the pre-treatment chamber of the spectrometer, C was detected on the surface. However, the C relative concentration was lower (C/[C + Pd] = 0.02) than in the PdRu sample. This could be explained as a consequence of the removal of carbon during the annealing up to 500 °C in H_2 stream.

3.4. PdRu film on porous stainless steel support

After synthesis optimization of the bimetallic films, PdRu co-deposition was performed using the most suitable conditions on top of the porous disc support until about 20 μm thick membrane was achieved. After PdRu membrane synthesis, the membrane was cut and characterized by SEM in order to study film adhesion and morphology of the binary film supported on top of the porous substrate.

Fig. 10 shows the top (a) and cross-section (b) view micrographs of the PdRu membrane deposited on top of a porous disc stainless steel 316L 0.2 μm grade (PdRu/0.2 μm PSSD). The membrane thickness obtained by SEM was 22 μm. Both micrographs show a homogeneous and pinhole-free morphology. A continuous and dense film was observed in the SEM cross-section view showed in two magnifications (Fig. 10b). These results were in agreement with the conditions chosen in the optimization stage.

To evaluate the hydrogen permeation properties of the metallic films synthesized in this study, a PdRu film was deposited on top of a porous stainless steel tubular support of 0.1 μm grade (PdRu/0.1 μm PSST). Fig. 11a shows the H_2 permeation flux during the annealing at 500 °C with a trans-membrane pressure of 10 kPa. The membrane showed a stable flux in the last 80 h of a total period of 120 h, achieving a flux equal to 3.8×10^{-3} mol s^{-1} m^{-2}. After the annealing stage, hydrogen fluxes were measured at several temperatures between 350 °C and 450 °C, as a function of the

Table 2
XPS and EDS data of the PdRu samples.

Sample	Temperature (°C)	%Ru[c]	%Ru[d]	Pd $3d_{5/2}$ (eV)[d]	Ru $3d_{5/2}$ (eV)[d]	$\%Ru_{Bulk}$ [e]
PdRu 1	40	2.5	0.4	335.4	280.1	–
PdRu 2	50 (0 rpm)	2.9	0.5	335.2	279.9	2.5
PdRu 3	70	3.1	0.5	335.4	280.1	–
PdRu 4	50 (800 rpm)	3.2	0.5	335.2	280.1	4.0
Pd[a]	–		–	335.1	–	–
Ru[b]	–		–	–	279.9	–

[a] Reference sample prepared by electroless plating.
[b] Ref. [37].
[c] PdRu sample prepared by electroless plating without annealing.
[d] After the treatment in H_2/Ar at 400 °C/10 min in the pre-treatment chamber.
[e] Bulk composition of Ruthenium obtained by EDS.

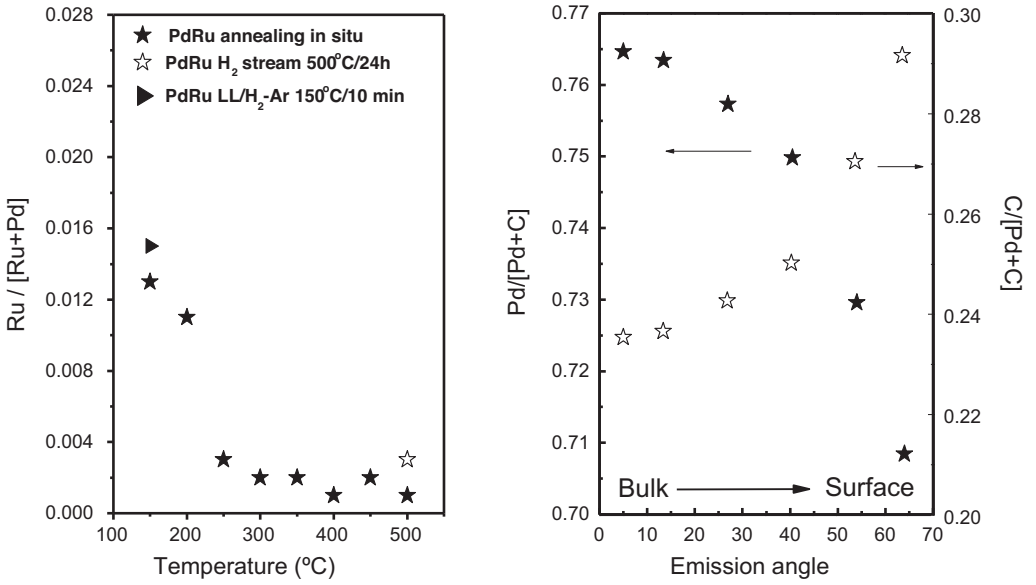

Fig. 9. (a) Ru surface composition of the PdRu sample as a function of the in situ annealing temperature and (b) Pd surface composition of the PdRu sample after the in situ annealing at 450 °C as a function of the emission angle.

trans-membrane pressure. Fig. 11b presents the hydrogen fluxes as a function of $(P_{Ret}{}^{0.5} - P_{Per}{}^{0.5})$; where "$P_{Ret''}$: retentate pressure and "$P_{Per''}$: the permeate pressure. The hydrogen flux shows a linear variation with $(P_{Ret}{}^{0.5} - P_{Per}{}^{0.5})$ at all temperatures, which reflects the diffusion of H_2 as the limiting step, as described by Sieverts' law. No nitrogen flow was detected with a bubble flowmeter up to a trans-membrane pressure of 100 kPa. The ideal selectivity, defined as the ratio between the flow of pure H_2 and N_2, was higher than 1700. An activation energy of 14.3 kJ mol^{-1} was estimated by the Arrhenius plot. The activation energy obtained for the PdRu membrane was similar to other Pd [41,42] and PdAg [22,43–45] membranes reported in the literature.

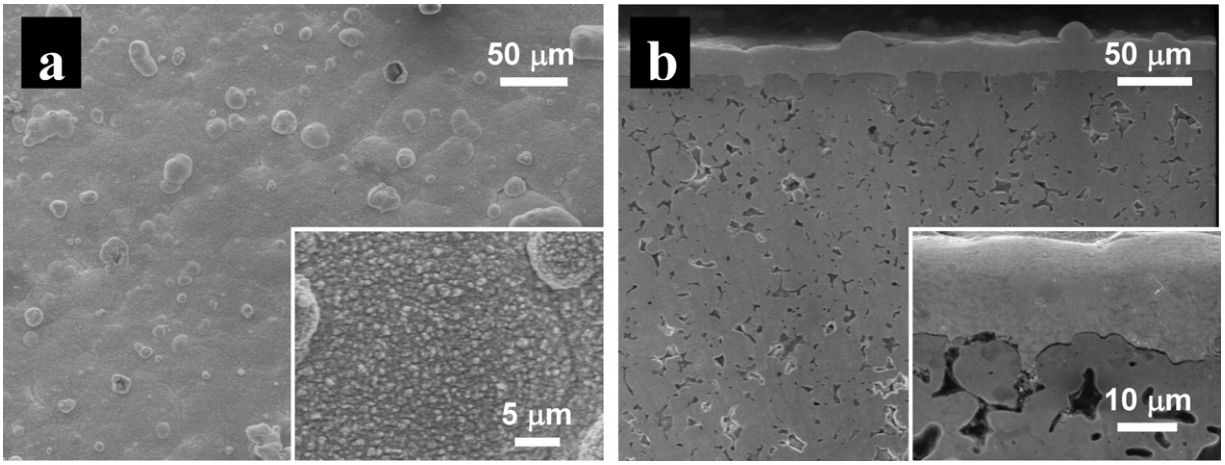

Fig. 10. (a) SEM top view of the PdRu/0.2 μm PSSD and (b) cross-section view of the PdRu/0.2 μm PSSD. Synthesis conditions: [Pd + Ru] = 10 mM, [Ru] = 1 mM, T = 50 °C, $[N_2H_4]$ = 30 mM, [EDTA] = 180 mM, pH = 11.5.

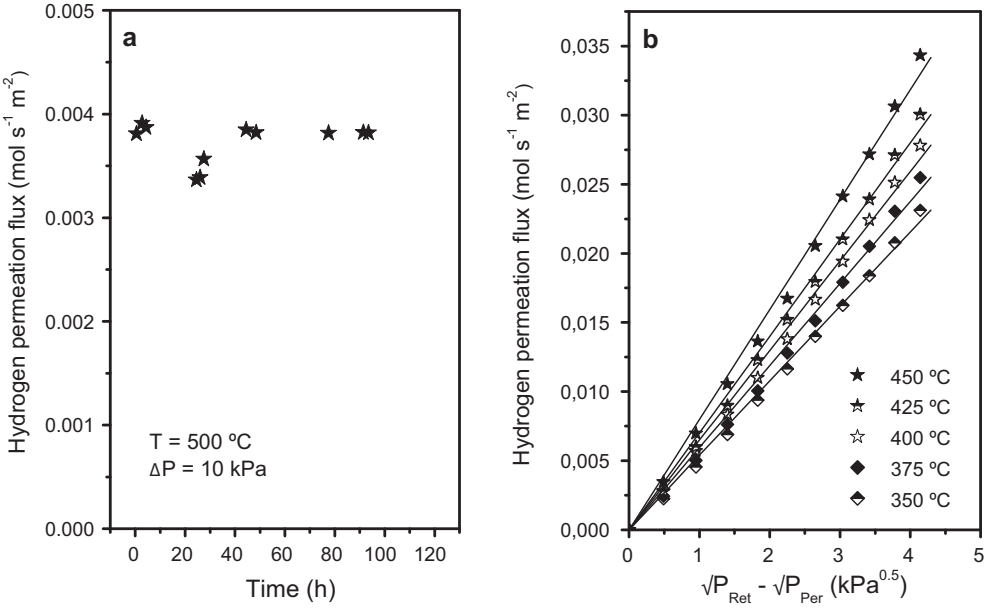

Fig. 11. H_2 flux through the PdRu/0.1 μm PSST membrane: (a) as a function of the time in the annealing stage, $\Delta P = 10$ kPa, $T = 500\,^{\circ}C$ and (b) as a function of pressure difference at several temperatures.

Previous publications [8,10] reported higher PdRu membrane permeabilities compared with the PdRu membrane synthesized in this work (6.5×10^{-9} mol m^{-1} s^{-1} Pa$^{-0.5}$). Way and co-workers [8] reported a permeability of 1.33×10^{-8} mol m^{-1} s^{-1} Pa$^{-0.5}$ for a $Pd_{90}Ru_{10}$ membrane synthesized by electroless co-deposition without employing carbon-containing complexing agents, to reduce the carbon contamination in the alloy film. On the other hand, for a non-alloy PdRu membrane synthesized by sequential electroless deposition, Ryi et al. [10] reported hydrogen permeability about 1.4 higher than the permeability of Pd. The lower hydrogen permeability of our membrane compared with other PdRu composites reported in the literature could be due to carbon contamination from EDTA of the plating bath.

4. Conclusions

In the optimization stage, the influence of synthesis variables of the PdRu electroless co-deposition on morphology, substrate adherence and bulk and surface composition were investigated. The pH plating bath study between 11.50 and 14.00 showed thinner metal films, more heterogeneous and less adherence increasing the pH. The films synthesized in an EDTA-free plating bath presented an improvement in the efficiency of the deposition but they also presented heterogeneous and dendritic morphologies. The optimum results were obtained in the 50–60 °C temperature range in the PdRu membrane synthesis. XPS studies showed strong Pd surface segregation in annealed PdRu membranes.

Defect-free PdRu films were synthesized by simultaneous electroless plating employing baths at pH 11.5, high concentration of hydrazine using EDTA as a stabilizer and temperatures near 50 °C. Under these conditions homogenous films, high deposition rates and good substrate adhesion were obtained. These results are of great importance in the synthesis of bimetallic PdRu membranes for hydrogen separation. The PdRu/0.1 μm PSST membrane showed good performance with a hydrogen permeability of 6.5×10^{-9} mol m^{-1} s^{-1} Pa$^{-0.5}$ and a selectivity higher than 1700.

Acknowledgments

The authors wish to acknowledge the financial support received from UNL, CONICET and ANPCyT. They are also grateful to ANPCyT for Grant PME 8-2003 to purchase the UHV Multi Analysis System. Thanks are given to Elsa Grimaldi for the English language editing.

References

[1] C.-H. Chen, Y.H. Ma, The effect of H_2S on the performance of Pd and Pd/Au composite membrane, J. Membr. Sci. 362 (2010) 535–544.
[2] L. Shi, A. Goldbach, G. Zeng, H. Xu, Preparation and performance of thin-layered PdAu/ceramic composite membranes, Int. J. Hydrogen Energy 35 (2010) 4201–4208.
[3] C.P. O'Brien, B.H. Howard, J.B. Miller, B.D. Morreale, A.J. Gellman, Inhibition of hydrogen transport through Pd and $Pd_{47}Cu_{53}$ membranes by H_2S at 350 °C, J. Membr. Sci. 349 (2010) 380–384.
[4] J. Okazaki, D.A. Pacheco Tanaka, M.A. Llosa Tanco, Y. Wakui, F. Mizukami, T.M. Suzuki, Hydrogen permeability study of the thin Pd–Ag alloy membranes in the temperature range across the α–β phase transition, J. Membr. Sci. 282 (2006) 370–374.
[5] K. Okuno, Application of electroless Ru deposits for electronics materials, Plat. Surf. Finish. 77 (1990) 48–52.
[6] G.O. Mallory, J.B. Hajdu, Electroless Plating – Fundamentals and Applications, American Electroplaters and Surface Finishers Society, New York, 1990.
[7] A.P. Mishchenko, M.E. Sarylova, I.A. Litvinov, L.I. Bezruk, V.M. Gryaznov, Influence of heat-treatment conditions on formation of pore structure of surface layer of palladium–ruthenium alloy foil, Russ. Chem. Bull. 34 (1985) 475–478.
[8] S.K. Gade, M.K. Keeling, A.P. Davidson, O. Hatlevik, J.D. Way, Palladium–ruthenium membranes for hydrogen separation fabricated by electroless co-deposition, Int. J. Hydrogen Energy 34 (2009) 6484–6491.
[9] N. Pomerantz, Y.H. Ma, Effect of H_2S on the performance and long-term stability of Pd/Cu membranes, Ind. Eng. Chem. Res. 48 (2009) 4030–4039.
[10] S.-K. Ryi, A. Li, C.J. Lim, J.R. Grace, Novel non-alloy Ru/Pd composite membrane fabricated by electroless plating for hydrogen separation, Int. J. Hydrogen Energy 36 (2011) 9335–9340.
[11] L. Wang, R. Yoshiie, S. Uemiya, Fabrication of novel Pd–Ag–Ru/Al_2O_3 ternary alloy composite membrane with remarkably enhanced H_2 permeability, J. Membr. Sci. 306 (2007) 1–7.
[12] S.W. Nam, S.P. Yoon, H.Y. Ha, S. Hong, A.P. Maganyuk, Methane steam reforming in a Pd–Ru membrane reactor, Korean J. Chem. Eng. 17 (2000) 288–291.
[13] L. Paturzo, F. Gallucci, A. Basile, P. Pertici, N. Scalera, G. Vitulli, Partial oxidation of methane in a catalytic ruthenium membrane reactor, Ind. Eng. Chem. Res. 42 (2003) 2968–2974.
[14] V.M. Gryaznov, O.S. Serebryannikova, Y.M. Serov, M.M. Ermilova, A.N. Karavanov, A.P. Mischenko, N.V. Orekhova, Preparation and catalysis over palladium composite membranes, J. Membr. Sci. 77 (1993) 284.

[15] S. Uemiya, T. Matsuda, E. Kikuchi, Hydrogen permeable palladium–silver alloy membrane supported on porous ceramics, J. Membr. Sci. 56 (1991) 315–325.
[16] J. Tong, R. Shirai, Y. Kashima, Y. Matsumura, Preparation of a pinhole-free Pd–Ag membrane on a porous metal support for pure hydrogen separation, J. Membr. Sci. 260 (2005) 84–89.
[17] M.L. Bosko, D. Yepes, S. Irusta, P. Eloy, P. Ruiz, E.A. Lombardo, L.M. Cornaglia, Characterization of Pd–Ag membranes after exposure to hydrogen flux at high temperatures, J. Membr. Sci. 306 (2007) 56–65.
[18] W.-H. Lin, H.-F. Chang, Characterizations of Pd–Ag membrane prepared by sequential electroless deposition, Surf. Coat. Technol. 194 (2005) 157–166.
[19] J.N. Keuler, L. Lorenzen, R.D. Sanderson, V. Prozesky, W.J. Przybylowicz, Characterization of electroless plated palladium–silver alloy membranes, Thin Solid Films 347 (1999) 91–98.
[20] Y.S. Cheng, K.L. Yeung, Palladium–silver composite membranes by electroless plating technique, J. Membr. Sci. 158 (1999) 127–141.
[21] J. Shu, B.P.A. Grandjean, E. Ghali, S. Kaliaguine, Simultaneous deposition of Pd and Ag on porous stainless steel by electroless plating, J. Membr. Sci. 77 (1993) 181–195.
[22] J.R. Brenner, G. Bhagat, P. Vasa, Hydrogen purification with palladium and palladium alloys on porous stainless steel membranes, Int. J. Oil Gas Coal Technol. 1 (2008) 109–125.
[23] H.-I. Chen, C.-Y. Chu, T.-C. Huang, Characterization of $PdAg/Al_2O_3$ composite membrane by electroless co-deposition, Thin Solid Films 460 (2004) 62–71.
[24] D.A. Pacheco Tanaka, M.A. Llosa Tanco, S.-i. Niwa, Y. Wakui, F. Mizukami, T. Namba, T.M. Suzuki, Preparation of palladium and silver alloy membrane on a porous a-alumina tube via simultaneous electroless plating, J. Membr. Sci. 247 (2005) 21–27.
[25] D. Yepes, L.M. Cornaglia, S. Irusta, E.A. Lombardo, Different oxides used as diffusion barriers in composite hydrogen permeable membranes, J. Membr. Sci. 274 (2006) 92–101.
[26] M.E. Ayturk, E.E. Engwall, Y.H. Ma, Microstructure analysis of the intermetallic diffusion-induced alloy, Ind. Eng. Chem. Res. 46 (2007) 4295–4306.
[27] M.E. Ayturk, Y.H. Ma, Electroless Pd and Ag deposition kinetics of the composite Pd and Pd/Ag membranes synthesized from agitated plating baths, J. Membr. Sci. 330 (2009) 233–245.
[28] A. Li, J.R. Grace, C.J. Lim, Preparation of thin Pd-based composite membrane on planar metallic substrate: Part I: Pre-treatment of porous stainless steel substrate, J. Membr. Sci. 298 (2007) 175–181.
[29] Y.H. Ma, B.C. Akis, M.E. Ayturk, F. Guazzone, E.E. Enqwall, I.P. Mardilovich, Characterization of intermetallic diffusion barrier and alloy formation for Pd/Cu and Pd/Ag porous stainless steel composite membranes, Ind. Eng. Chem. Res. 43 (2004) 2936–2945.
[30] L.M. Bosko, J.B. Miller, E.A. Lombardo, A. Gellman, L.M. Cornaglia, Surface characterization of Pd–Ag composite membranes after annealing at various temperatures, J. Membr. Sci. 369 (2011) 267–276.
[31] K.L. Yeung, S.C. Christiansen, A. Varma, Palladium composite membranes by electroless plating technique: relationships between plating kinetics, film microstructure and membrane performance, J. Membr. Sci. 159 (1999) 107–122.
[32] R. Bhandari, Y.H. Ma, Pd–Ag membrane synthesis: the electroless and electroplating conditions and their effect on the deposits morphology, J. Membr. Sci. 334 (2009) 50–63.
[33] M. Dogan, S. Kilicarslan, Effects of process parameters on the synthesis of palladium membranes, Nucl. Instr. Methods Phys. Res. B 266 (2008) 3458–3466.
[34] B.D. Cullity, S.R. Stock, Elements of X-ray Diffraction, 3rd ed., Prentice-Hall, 2001.
[35] A.M. Tarditi, L.M. Cornaglia, Novel PdAgCu ternary alloy as promising materials for hydrogen separation membranes: synthesis and characterization, Surf. Sci. 605 (2011) 62–71.
[36] W. Mekonnen, B. Arstad, H. Klette, J.C. Walmsley, R. Bredesen, H. Benvik, R. Holmestad, Microstructural characterization of self-supported 1.6 μm Pd/Ag membranes, J. Membr. Sci. 310 (2008) 337–348.
[37] C. Mun, J.J. Ehrhardt, J. Lambert, C. Madic, XPS investigations of ruthenium deposited onto representative inner surfaces of nuclear reactor containment buildings, Appl. Surf. Sci. 253 (2007) 7613–7621.
[38] Y. Sakamoto, F.L. Chen, Y. Kinari, F. Sakamoto, Effect of carbon monoxide on hydrogen permeation in some palladium-based alloy membranes, Int. J. Hydrogen Energy 210 (1996) 1017–1024.
[39] F. Gallucci, F. Chiaravalloti, S. Tosti, E. Drioli, A. Basile, The effect of mixture gas on the hydrogen permeation through a palladium membrane: experimental studies and theoretical approach, Int. J. Hydrogen Energy 32 (2007) 1837–1845.
[40] R.J. Wrobel, S. Becker, Carbon and sulphur on Pd (1 1 1) and Pt (1 1 1): experimental problems during cleaning of the substrates and impact of sulphur on the redox properties of CeO_x in the CeO_x/Pd (1 1 1) system, Vacuum 84 (2010) 1258–1265.
[41] I.P. Mardilovich, Y. She, Y.H. Ma, M.H. Rei, Defect-free palladium membranes on porous stainless-steel support, AIChE J. 44 (1998) 310–322.
[42] K.S. Rothenberger, The permeability of hydrogen in bulk palladium at elevated temperatures and pressures, J. Membr. Sci. 212 (2003) 87–97.
[43] E.L. Foletto, J.V. Wirbitzki da Silveira, S.L. Jahn, Preparation of palladium–silver alloy membranes for hydrogen permeation, Latin Am. Appl. Res. 38 (2008) 79–84.
[44] J. Tong, L. Su, Y. Kashima, R. Shirai, H. Suda, Y. Matsumura, Simultaneously depositing Pd–Ag thin membrane on asymmetric porous stainless steel tube and application to produce hydrogen from steam reforming of methane, Ind. Eng. Chem. Res. 45 (2006) 648–655.
[45] K. Zhang, X. Wei, Z. Rui, Y. Li, Y.S. Lin, Effect of metal–support interface on hydrogen permeation through palladium membranes, AIChE J. 55 (2009) 630–639.